Center for Turbulence Research
Proceedings of the Summer Program 1994

Numerical investigation of supersonic turbulent boundary layers with high wall temperature

By Y. Guo[1] AND N. A. Adams[2]

A direct numerical approach has been developed to simulate supersonic turbulent boundary layers. The mean flow quantities are obtained by solving the parabolized Reynolds-averaged Navier-Stokes equations (globally). Fluctuating quantities are computed locally with a temporal direct numerical simulation approach, in which nonparallel effects of boundary layers are partially modeled. Preliminary numerical results obtained at the free-stream Mach numbers 3, 4.5, and 6 with hot-wall conditions are presented. Approximately 5 million grid points are used in all three cases. The numerical results indicate that compressibility effects on turbulent kinetic energy, in terms of dilatational dissipation and pressure-dilatation correlation, are small. Due to the hot-wall conditions the results show significant low Reynolds number effects and large streamwise streaks. Further simulations with a bigger computational box or a cold-wall condition are desirable.

1. Introduction

Studies of compressible turbulent boundary layer flows are of fundamental interest. Understanding of such flows, particularly the effects of compressibility on turbulence, may help to improve turbulence models used in many industrial applications. Over the years, many experimental efforts have been made (cf. Spina *et al.*, 1994), and a great deal of knowledge has been obtained about these flows. But due to the difficulties encountered in high speed flow experiments, many aspects of these flows still remain unclear (cf. Lele, 1994 and Spina *et al.*, 1994). Recently with the rapid increase of computing power, direct numerical simulation (DNS) has become one alternative tool to investigate these flows. In this study, we present our first effort in this direction. Preliminary results from three case studies at Mach numbers 3, 4.5, and 6 are reported.

The problem in this study is the compressible turbulent boundary layer flow over a flat plate. We consider a region after the leading edge, where the flow is free of the shock caused by the leading edge and the boundary layer forms over the wall and grows in the streamwise direction. Generally, there are two ways to do DNS of boundary layer flows: spatial DNS and temporal DNS (cf. Kleiser & Zang, 1991 for a review). A spatial DNS approach (SDNS) is the closest numerical realization of a turbulent boundary layer experiment, but it demands an enormous amount

1 DLR, Institute for Fluid Mechanics, Germany. Current address: Institute of Fluid Dynamics, ETH Zürich, Switzerland.

2 Center for Turbulence Research

of computing resources and therefore is prohibitively expensive, especially in the case of compressible boundary layer flows. So far its application has been limited to producing a few benchmark data (Spalart & Watmuff, 1993). A temporal DNS approach (TDNS), where the flow is assumed to be locally parallel and develops in time, is highly efficient and requires no inflow and outflow boundary conditions (cf. Kleiser & Zang, 1991). It has been applied successfully to the direct simulations of turbulent channel flows (cf. Kim *et al.*, 1987, Coleman *et al.*1993) and has provided considerable details and insights about the turbulence in these flows. But due to the use of the parallel flow assumption in its formulation, its applications to turbulent boundary layers have suffered certain drawbacks. Firstly, the mean flow quantities do not satisfy the Navier-Stokes equations and always exhibit undesirable temporal growth. Secondly, the nonparallel effects of a turbulent boundary layer cannot be considered. To overcome these problems, Spalart & Leonard (1985) and Spalart (1986) assumed self-similarity both for the mean velocity and for the Reynolds stresses in their studies of equilibrium turbulent boundary layers and sink flows. This assumption is reasonable, but is strictly justified only in the case of sink flows. In Spalart (1988), a more general approach was developed using a multiple-scale analysis to approximate the local effects of the streamwise growth of the flow. Satisfactory results have been obtained for boundary layer flows on a flat plate.

However, a direct application of Spalart's multiple-scale analysis (1988) to compressible flow is rather tedious and difficult, due to many nonlinear terms in the compressible Navier-Stokes equations. In order to avoid this problem, a different approach has been used in this study. In the following section, we present the details of this approach, together with discussions concerning its application to more general cases. Brief comments on the numerical implementation and validation of this approach are given in §3. In §4, we present preliminary numerical results of turbulent boundary layers at $M_\infty = 3$, 4.5, and 6. Concluding remarks are given in §5.

2. Numerical method

It is known that there exist two different scales in a turbulent boundary layer: mean flow quantities exhibit large scales and slow variations in the streamwise direction, while turbulence quantities are generally of small scale and fast variation (cf. Spalart, 1988). In some sense, mean flow quantities can be viewed as global quantities, carrying upstream information downstream. For example, the downstream profiles of mean flow quantities depend on the upstream profiles of these quantities. Therefore these quantities cannot be solved by any local procedure without resorting to any similarity assumption (note that a TDNS approach is a local procedure). Turbulence quantities, on the other hand, are generally "local", being generated and dissipated within short time and small space. Intuitively, one would expect that it would be more efficient to compute these two different scales with different numerical approaches.

Motivated by the above observation, we developed an approach which computes the turbulence quantities locally with a TDNS approach, and computes the mean

flow quantities globally by solving the Reynolds-averaged Navier-Stokes equations. This approach is formulated in such a way that it allows the solutions of the Reynolds-averaged Navier-Stokes equations be marched downstream spatially using the Reynolds stresses, which are computed locally at each spatial step by a TDNS approach. Special care has been taken to include the nonparallel effects of the turbulent boundary layer flows into the TDNS approach, which is a natural extension of our earlier work on TDNS of growing transitional boundary layers (Guo *et al.*, 1994).

2.1 Solving Reynolds-averaged equations for mean flow quantities within TDNS

For simplicity, we first demonstrate our numerical approach using an incompressible boundary layer flow as an example. Application of this approach to compressible flow is presented in §2.3. In this report, we designate x as the streamwise direction, y as the spanwise direction, and z as the wall-normal direction. Vector notations are preferred due to irregular terms introduced by parabolization procedures.

For any turbulent boundary layer flow, the flow field can be decomposed as

$$\mathbf{u} = \mathbf{u}^0 + \mathbf{u}' \,, \tag{1}$$

where $\mathbf{u}^0$ represents the stationary part, which usually includes the mean flow, $\mathbf{u}_0^0$ (i.e. $(0,0)$ mode), and all stationary streamwise vortices, $\mathbf{u}_1^0$ (i.e. $(0,k_y)$ modes, $k_y \neq 0$). The term $\mathbf{u}'$ represents the remaining part which fluctuates with time. The governing equations for $\mathbf{u}^0$ are the Reynolds averaged Navier-Stokes equations (in dimensionless form):

$$\nabla \cdot (\mathbf{u}^0 \mathbf{u}^0) = -\nabla p^0 + \frac{1}{Re} \nabla^2 \mathbf{u}^0 - \nabla \cdot (\overline{\mathbf{u}'\mathbf{u}'}) \,, \tag{2}$$

$$\nabla \cdot \mathbf{u}^0 = \mathbf{0} \,, \tag{3}$$

where $\mathbf{u}'\mathbf{u}'$ are the well-known Reynolds stresses, and an overline represents a time-averaged quantity. In boundary layers, $\mathbf{u}^0$ usually has slow variation in the streamwise direction, thus the governing Eqs. (2) and (3) can be parabolized (cf. Fletcher, 1988 and Guo & Finlay, 1994): the term ∇^2 is replaced by ∇_P^2,

$$\nabla_P^2 = \frac{\partial^2}{\partial y^2} + \frac{\partial^2}{\partial z^2} \,, \tag{4}$$

and the pressure p^0 in the $x-$momentum equation is replaced by the mean pressure averaged across the $y-z$ plane, p_0^0. The solutions of the resulting equations then can be marched downstream efficiently using a spatial marching scheme. Parabolization procedures for more general cases can be found in Fletcher (1988).

One important issue in solving the parabolized version of (2) and (3) is the numerical treatment of the Reynolds stress terms. In a turbulent boundary layer, these are the dominant terms, and it is desirable to treat these terms implicitly in spatial marching schemes in order to avoid any severe restriction on spatial marching step sizes. Since the Reynolds stress terms are computed by a TDNS approach in this

study, they cannot be expressed explicitly in terms of $\mathbf{u}^0$. Thus an efficient way has to be found to deal with these terms implicitly.

It can be shown that in a conventional TDNS approach, the actual equations solved for $\mathbf{u}^0$ are:

$$\frac{\partial \mathbf{u}^0}{\partial t} + \nabla_P \cdot (\mathbf{u}^0 \mathbf{u}^0) = -\nabla_P p^0 + \frac{1}{Re} \nabla_P^2 \mathbf{u}^0 - \nabla_P \cdot (\overline{\mathbf{u}'\mathbf{u}'}) \,, \tag{5}$$

$$\frac{\partial \mathbf{u}^0}{\partial t} + \nabla_P \cdot \mathbf{u}^0 = \mathbf{0} \,. \tag{6}$$

Note that in (5-6), $\mathbf{u}^0$ is a function of time and an overline represents a *spatial-averaged* quantity. Compared to the parabolized (2-3), the following term is missing from the right hand sides of (5-6):

$$\mathbf{Z_0} = (z_{01}, z_{02}, z_{03}, z_{04})^T \,, \tag{7}$$

where

$$\begin{aligned}
z_{01} &= -\frac{\partial u^0 u^0}{\partial x} - \frac{\partial p_0^0}{\partial x} - \frac{\partial \overline{u'u'}}{\partial x} \,, \\
z_{02} &= -\frac{\partial u^0 v^0}{\partial x} - \frac{\partial \overline{u'v'}}{\partial x} \,, \\
z_{03} &= -\frac{\partial u^0 w^0}{\partial x} - \frac{\partial \overline{u'w'}}{\partial x} \,, \\
z_{04} &= -\frac{\partial u^0}{\partial x} \,.
\end{aligned}$$

Assuming spatial-averaged quantities are good approximations to time-averaged quantities, Eqs. (5-6), with the missing term (7) added, constitute a transient problem of the parabolized (2-3). The solutions of these equations converge to those of the parabolized (2-3) when $\partial \mathbf{u}^0 / \partial t \to \mathbf{0}$. Note that the term $\mathbf{Z_0}$ only acts on the governing equations for $\mathbf{u}^0$. The streamwise variation of the Reynolds stress terms are also included in (7).

To further demonstrate how Eqs. (5-6) are solved in a TDNS together with the term $\mathbf{Z_0}$, we discretize the $x-$momentum equation in the x direction with an Euler implicit scheme:

$$\begin{aligned}
\frac{\partial {u^0}_{n+1}}{\partial t} = &-\frac{\partial (u^0 v^0)_{n+1}}{\partial y} - \frac{\partial (u^0 w^0)_{n+1}}{\partial z} + \frac{1}{Re}\left(\frac{\partial^2 {u^0}_{n+1}}{\partial y^2} + \frac{\partial^2 {u^0}_{n+1}}{\partial z^2}\right) \\
&- \left(\frac{\partial (\overline{u'v'})_{n+1}}{\partial y} + \frac{\partial (\overline{u'w'})_{n+1}}{\partial z}\right) - \frac{(u^0 u^0)_{n+1} - (u^0 u^0)_n}{\Delta x_{n+1}} \\
&- \frac{p^0_{0\,n+1} - p^0_{0n}}{\Delta x_{n+1}} - \frac{(\overline{u'u'})_{n+1} - (\overline{u'u'})_n}{\Delta x_{n+1}} \,,
\end{aligned} \tag{8}$$

where a subscript "$n+1$" denotes the solution evaluated at the downstream location $x = x_{n+1}$, and $\Delta x_{n+1} = x_{n+1} - x_n$. At each station $x = x_{n+1}$, the solution of (8)

is iterated in time until a steady-state solution is reached. Then the solution of (8) is marched spatially to the next station $x = x_{n+2}$. In practice, we find high order backward-differentiation-formulas (BDF) with variable step sizes (cf. Hairer *et al.*, 1987) are rather satisfactory: these schemes with accuracy up to sixth order are unconditionally stable, and the implementation only involves the term $\mathbf{Z}_0$ in an existing TDNS code. In our code, a second order BDF is used:

$$\frac{\partial(\ )}{\partial x} = \frac{1}{x_{n+1} - x_n}\left[\frac{1+2\omega_n}{1+\omega_n}(\ )_{n+1} - (1+\omega_n)(\ )_n + \frac{\omega_n^2}{1+\omega_n}(\ )_{n-1}\right], \tag{9}$$

where $\omega_n = (x_{n+1} - x_n)/(x_n - x_{n-1})$.

2.2 Computing turbulence quantities with TDNS: nonparallel effects

Turbulence quantities in boundary layers are not homogeneous locally in the x direction. When a TDNS approach is used to compute these quantities, the issue of nonparallel effects arises. In Guo *et al.* (1994), we have discussed extensively this issue in the case of transitional flows. Here we adopt a similar methodology. The basic idea of this approach is as follows: we assume that the nonparallel flow $\mathbf{u}$ can be decomposed as the perturbation expansion:

$$\mathbf{u} = \mathbf{u}_0 + \mathbf{u}_1\epsilon + \mathbf{u}_2\epsilon^2 + \cdots, \tag{10}$$

where $\mathbf{u}_i$ $(i = 0, 1, 2, \cdots)$ are periodic functions in both x and y, and ϵ is some perturbation parameter. Substituting Eq. (10) into the Navier-Stokes equations, we can derive one set of equations for each power i of the parameter ϵ. These equation sets all have the periodic functions $\mathbf{u}_i$ as unknowns. In a sense, the original nonperiodic system has been decomposed into periodic subsystems, where then Fourier schemes can be used. If Eq. (10) is truncated at $i = n-1$, the approximation error is given by

$$\delta = \mathbf{u}_n\epsilon^n + \mathbf{u}_{n+1}\epsilon^{n+1} + \cdots . \tag{11}$$

If δ is bounded and decays with n, then Fourier schemes can be used to obtain the solution of a nonparallel system. In Guo *et al.* (1994), we have shown that the decomposition (10) can be obtained for transitional boundary layer flows, and Eq. (11) is bounded and decays with n.

For a turbulent boundary layer, we can perform the following analysis. Following Spalart (1988), $\mathbf{u}$ can be decomposed as

$$\mathbf{u} = \mathbf{u}^0 + \mathbf{u}' = \mathbf{u}^0 + \mathbf{A}(x,z)\mathbf{B}(x,y,z,t) , \tag{12}$$

where $\mathbf{u}^0$ represents mean flow quantities, and $\mathbf{A}(x,z)$ is the "amplitude function", which is proportional to the r.m.s. of $\mathbf{u}$. Both $\mathbf{u}^0$ and $\mathbf{A}(x,z)$ have slow variations in the x directions. The term $\mathbf{B}(x,y,z,t)$ represents the fast fluctuating part. Taylor-expanding $\mathbf{u}^0$ and $\mathbf{A}(x,z)$ in the neighborhood of x_0, we have

$$\mathbf{u}^0(x,z) = \mathbf{u}^0(x_0,z) + \frac{\partial \mathbf{u}^0}{\partial x}(x - x_0) + \frac{1}{2!}\frac{\partial^2 \mathbf{u}^0}{\partial x^2}(x - x_0)^2 + \cdots , \tag{13}$$

$$\mathbf{A}(x,z) = \mathbf{A}(x_0,z) + \frac{\partial \mathbf{A}}{\partial x}(x-x_0) + \frac{1}{2!}\frac{\partial^2 \mathbf{A}}{\partial x^2}(x-x_0)^2 + \cdots . \tag{14}$$

We denote the length scale of the fluctuating part $\mathbf{B}(x,y,z,t)$ as l, and the length scale of the mean flow quantities as L. Assuming that $\partial/\partial x$ can be scaled with L and $x - x_0$ with l, we have the expansions (13-14) decay asymptotically at a rate $O(l/L)^n/n!$.

In Spalart (1988), $\mathbf{B}(x,y,z,t)$ was assumed to be periodic in the x direction. More generally, we can assume that

$$\mathbf{B}(x,y,z,t) = \mathbf{B}_0 + \mathbf{B}_1(x-x_0) + \mathbf{B}_2(x-x_0)^2 + ..., \tag{15}$$

where $\mathbf{B}_j$ $(j = 0, 1, \cdots)$ are periodic in both x and y. Generally, we can assume that $\mathbf{B}_{i-1}$ is one order smaller than $\mathbf{B}_i$. Note that this assumption cannot be proved theoretically, but it is less restrictive than assuming $\mathbf{B}$ to be periodic. Substituting (13-15) into (12), one can show that $\mathbf{u}'$ can be written in the form of

$$\mathbf{u}' = \mathbf{u}'_0 + \mathbf{u}'_1(x-x_0) + \mathbf{u}'_2(x-x_0)^2 + \cdots , \tag{16}$$

where $\mathbf{u}'_j$ $(j = 0, 1, \cdots)$ are periodic in x and y, and $\mathbf{u}'_i$ is generally one order larger than $\mathbf{u}'_{i-1}$. Then the error defined by (11) is bounded and decays with n.

Due to the complexity, only the first set of equations $(i = 0)$ are considered in this study. The derivative of $\mathbf{u}$ is approximated by

$$\frac{\partial \mathbf{u}}{\partial x} \approx \frac{\partial \mathbf{u}^0}{\partial x} + \frac{\partial \mathbf{u}'_0}{\partial x} + \mathbf{u}'_1 \tag{17}$$

For a turbulent boundary layer, the nonparallel effect contributed by $\mathbf{u}'_1$ cannot be modeled due to the lack of information about $\mathbf{u}'_1$. In a transitional flow, this term can be partially modeled, and has been shown to be small in Guo *et al.* (1994). In a standard TDNS approach, the term $\partial \mathbf{u}^0/\partial x$ is zero, and thus the nonparallel effect contributed by this term is not considered. In this study, the nonparallel contribution of this term is considered by adding the following term to the right-hand side of the governing equations solved by a TDNS approach,

$$\mathbf{Z}_1 = (z_{11}, z_{12}, z_{13}, z_{14})^T , \tag{18}$$

where

$$\begin{aligned}
z_{11} &= -2(u-u^0)\frac{\partial u^0}{\partial x} , \\
z_{12} &= -(u-u^0)\frac{\partial v^0}{\partial x} - (v-v^0)\frac{\partial u^0}{\partial x} , \\
z_{13} &= -(u-u^0)\frac{\partial w^0}{\partial x} - (w-w^0)\frac{\partial u^0}{\partial x} , \\
z_{14} &= 0 .
\end{aligned}$$

The term $\mathbf{Z}_1$ is equivalent to the forcing term $\mathbf{Z}_1$ in Guo *et al.* (1994), and it only acts on the governing equations for $\mathbf{u}'$.

2.3 Application to compressible boundary flow

In the case of compressible boundary layer flows, the governing equations we have solved can be written in the dimensionless conservative form as:

$$\frac{\partial \mathbf{U}}{\partial t} = \frac{\partial \mathbf{F}}{\partial x} + \frac{\partial \mathbf{G}}{\partial y} + \frac{\partial \mathbf{H}}{\partial z} + \mathbf{Z}_0 + \mathbf{Z}_1 \ . \tag{19}$$

The vector $\mathbf{U}$ is the solution vector defined by $\mathbf{U} = (\rho, \rho u, \rho v, \rho w, E)^T$, where ρ is the density normalized with the free-stream density ρ^*_∞, and u, v, and w are the velocity components normalized with the free-stream velocity u^*_∞. Here, a subscript "∞" denotes the quantity evaluated at the freestream and an asterisk denotes a dimensional quantity. The total energy E is defined by

$$E = \frac{1}{\kappa - 1} p + \frac{\rho}{2}(u^2 + v^2 + w^2)$$

where κ is the ratio of specific heats and p is the pressure normalized with $\rho^*_\infty {u^*_\infty}^2$. The pressure p is related to the temperature T by a perfect-gas law

$$p \kappa M^2_\infty = \rho T \ .$$

Sutherland's law is used for the viscosity calculation. The vectors $\mathbf{F}$, $\mathbf{G}$ and $\mathbf{H}$ are the standard flux vectors in the x, y, and z directions respectively.

The term $\mathbf{Z}_0$ is derived in the same way as described early in §2.1. It has the following form:

$$\mathbf{Z}_0 = \frac{\partial}{\partial x} \begin{bmatrix} -\overline{\rho u} \\ -\overline{\rho u^2} - p^0_0 + (\overline{\tau_{xx}})_T \\ -\overline{\rho u v} + (\overline{\tau_{xy}})_T \\ -\overline{\rho u w} + (\overline{\tau_{xz}})_T \\ -\overline{u(E+p)} - (\overline{q_x})_T + (\overline{u \tau_{xx}})_T + (\overline{v \tau_{xy}})_T + (\overline{w \tau_{xz}})_T \end{bmatrix} + \mathbf{Z}_m \ , \tag{20}$$

where τ_{xx}, τ_{xy}, and τ_{xz} are the components of the shear stress tensor and q_x is the heat flux component in the x direction. Here an overline denotes a spatial-averaged quantity. A subscript "T" denotes the quantity been evaluated in a TDNS scheme. The term $\mathbf{Z}_m$ contains the terms missing in the terms $(\ )_T$, due to the use of Fourier schemes. It has a form of

$$\mathbf{Z}_m = (z_{1m}, z_{2m}, z_{3m}, z_{4m}, z_{5m})^T \ , \tag{21}$$

where

$$z_{1m} = 0 \ ,$$

$$z_{2m} = \frac{4}{3}\frac{\partial}{\partial x}\left(\frac{\bar{\mu}}{Re}\right)\frac{\partial \bar{u}}{\partial x} + \frac{\partial}{\partial y}\left(\frac{\bar{\mu}}{Re}\frac{\partial \bar{v}}{\partial x}\right) + \frac{\partial}{\partial z}\left(\frac{\bar{\mu}}{Re}\frac{\partial \bar{w}}{\partial x}\right) \ ,$$

$$z_{3m} = \frac{\partial}{\partial x}\left(\frac{\bar{\mu}}{Re}\right)\frac{\partial \bar{w}}{\partial x} - \frac{2}{3}\frac{\partial}{\partial y}\left(\frac{\bar{\mu}}{Re}\frac{\partial \bar{u}}{\partial x}\right) - \frac{2}{3}\frac{\partial}{\partial z}\left(\frac{\bar{\mu}}{Re}\frac{\partial \bar{u}}{\partial x}\right) ,$$

$$z_{4m} = \frac{\partial}{\partial x}\left(\frac{\bar{\mu}}{Re}\right)\frac{\partial \bar{v}}{\partial x} ,$$

$$\begin{aligned} z_{5m} = {} & \frac{1}{(\kappa-1)M_\infty^2 Pr}\frac{\partial}{\partial x}\left(\frac{\bar{\mu}}{Re}\right)\frac{\partial \bar{T}}{\partial x} + \frac{4}{3}\frac{\bar{\mu}}{Re}\left(\frac{\partial \bar{u}}{\partial x}\right)^2 + \frac{4}{3}\bar{u}\frac{\partial}{\partial x}\left(\frac{\bar{\mu}}{Re}\right)\frac{\partial \bar{u}}{\partial x} \\ & + \frac{\bar{\mu}}{Re}\left(\frac{\partial \bar{v}}{\partial x}\right)^2 + \bar{v}\frac{\partial}{\partial x}\left(\frac{\bar{\mu}}{Re}\right)\frac{\partial \bar{v}}{\partial x} + \frac{\bar{\mu}}{Re}\left(\frac{\partial \bar{w}}{\partial x}\right)^2 + \bar{w}\frac{\partial}{\partial x}\left(\bar{u}\frac{\bar{\mu}}{Re}\right)\frac{\partial \bar{v}}{\partial x} \\ & + \frac{\partial}{\partial y}\left(\frac{\bar{\mu}}{Re}\frac{\partial \bar{w}}{\partial x}\right) - \frac{2}{3}\frac{\partial}{\partial y}\left(\bar{v}\frac{\bar{\mu}}{Re}\frac{\partial \bar{u}}{\partial x}\right) + \frac{\partial}{\partial z}\left(\bar{u}\frac{\bar{\mu}}{Re}\frac{\partial \bar{w}}{\partial x}\right) - \frac{2}{3}\frac{\partial}{\partial z}\left(\bar{w}\frac{\bar{\mu}}{Re}\frac{\partial \bar{u}}{\partial x}\right) . \end{aligned}$$

It can be shown that $\mathbf{Z}_m$ is very small, and can be neglected. For completeness, we retain this term in our scheme.

Note that in Eq. (20), a parabolization procedure similar to the one described in Fletcher (1988) has been used: the pressure p in the $x-$momentum equation is first replaced by the mean pressure p_0^0; secondly, the mean pressure p_0^0 in the subsonic section of the boundary layer is extrapolated from the adjacent supersonic layer. For a boundary layer over a flat plate, we set $\partial p_0^0/\partial x$ to be zero.

The term $\mathbf{Z}_1$ in Eq. (19) is given by

$$\mathbf{Z}_1 = (z_{11}, z_{12}, z_{13}, z_{14}, z_{15})^T , \tag{22}$$

where

$$z_{11} = -\rho\frac{\partial u^0}{\partial x} - u\frac{\partial \rho^0}{\partial x} + \frac{\partial(\rho^2 u^0)}{\partial x} ,$$

$$z_{12} = -(u-u^0)\frac{\partial \overline{\rho u}}{\partial x} - (\rho u - \overline{\rho u})\frac{\partial u^0}{\partial x} ,$$

$$z_{13} = -(u-u^0)\frac{\partial \overline{\rho v}}{\partial x} - (\rho v - \overline{\rho v})\frac{\partial u^0}{\partial x} ,$$

$$z_{14} = -(u-u^0)\frac{\partial \overline{\rho w}}{\partial x} - (\rho w - \overline{\rho w})\frac{\partial u^0}{\partial x} ,$$

$$z_{15} = -(u-u^0)\frac{\partial}{\partial x}(E^0+p^0) - (E+p-E^0-p^0)\frac{\partial u^0}{\partial x} .$$

2.4 Some comments

It can be shown that the governing equations obtained from our approach for an incompressible boundary layer over a flat plate are identical to those of Spalart (1988) when the coordinate transformation in Spalart (1988) is not used. In a sense, our approach is similar to Spalart's (1988) in that in both two scales are utilized. In our approach, the long-scale analysis is explicitly applied to the *governing equations* for mean flow quantities (i.e. $(0, k_y)$ modes), and the short-scale analysis to the *governing equations* for turbulence quantities. When there are large streamwise streaks, e.g. in a three-dimensional boundary layer, our approach may be more

general since the related governing equations for mean flow quantities are explicitly parabolized, making the use of spatial marching schemes more justifiable.

In Spalart (1988), coordinate tilting has been introduced to model the nonparallel effects of boundary layers. In Guo *et al.* (1994), our experience with transitional compressible boundary layer flows shows that the coordinate transformation technique does not guarantee an improved result, partly due to the difficulty in selecting a proper tilting angle. In this study, this technique is not used.

Compared to the parabolized stability equations (PSE) approach developed for transitional flows (Bertolotti, Herbert & Spalart, 1991), we have the following comments. The PSE has been proven to be a very powerful tool in studying the transition process in spatially growing boundary layers up to the early stage of breakdown. The possibility of developing a PSE type approach for turbulent boundary layers has been appealing (Zang, 1991). To our understanding, the PSE relies on the spatial marching of shape functions (eigenfunctions) of all modes in the streamwise direction. This requires the spatial evolutions of all shape functions to be slow in this direction. In turbulent boundary layers, only the mean flow $\mathbf{u}_1^0$ and the stationary spanwise modes $\mathbf{u}_2^0$ have slowly evolving shape functions in the streamwise direction. The shape functions of other modes do not have slow variations in the streamwise direction, and thus cannot be marched downstream by a spatial marching scheme. The method we described in this study has explored the possibility of marching downstream the shape functions of $\mathbf{u}_1^0$ and $\mathbf{u}_2^0$, and computes the other modes locally. Thus it can be viewed as a version of PSE for turbulent boundary layer flows.

3. Implementation and code validation

The numerical method discussed in §2 has been implemented in a TDNS code developed by Adams (1993). Fourier collocation methods are employed for the spatial derivative calculations in the spanwise and streamwise directions, and a compact central finite-difference (Padé) scheme is employed in the non-periodic wall-normal direction. The solution is advanced in time fully explicitly by a third-order low-storage Runge-Kutta scheme. More details of this TDNS code can be found in Adams (1993).

In order to maintain flexibility, both streamwise and spanwise spatial-averaging can be performed on the quantities at x_{n+1}. For the quantities at x_n and x_{n-1}, time-averaging is also implemented as an option, since the spanwise modes $\mathbf{u}_2^0$ in some cases evolve with time t and a time-averaging is needed to obtain stationary solutions. In this study, spanwise spatial-averaging is not used.

In order to validate the code, we first simulate a laminar boundary layer flow at $M_\infty = 4.5$, with all non-zero streamwise modes set to be zero (i.e. the Reynolds stress terms are set to be zero). Similarity solutions for the boundary layer were used as the initial profiles to start the downstream spatial marching. At each spatial step, the solution is advanced in time until a steady-state solution is reached. Once the steady-state solution is achieved, the solution is marched downstream again one step. At all spatial steps, our code can duplicate the similarity solutions accurately.

Simulations of turbulent boundary layer flows cannot be validated directly due to the lack of comprehensive database for these flows. In the following section, we present preliminary results for the turbulent boundary layers at three different Mach numbers.

4. Preliminary results

4.1 Simulation parameters and procedures

In order to study the compressibility effects at different free-stream Mach number, we have done three case studies at $M_\infty = 3$, 4.5, and 6. The simulation parameters for these three cases are listed in Table 1. The sizes of the computational boxes, L_x in the x direction, L_y in the y direction, and L_z in the wall-normal direction, are given in the terms of both boundary layer thickness, δ_0, and wall unit. The numbers of grids in the x, y, and z directions are given by N_x, N_y, and N_z respectively. Sampling time t_s is non-dimensionalized by the free-stream variables. In all cases, the laminar adiabatic wall temperatures were used as the constant wall temperatures in the simulations, with $T_\infty = 61.15K$.

TABLE 1. Simulation parameters.

M_∞	Re_θ	T_w/T_∞	L_x	L_y	L_z	$N_x \times N_y \times N_z$	t_s
3	3015	2.5	$1.67\delta_0$	$0.96\delta_0$	$3.59\delta_0$	192×144×180	34
			527^+	300^+	1133^+		
4.5	2618	4.38	$1.59\delta_0$	$0.95\delta_0$	$3.18\delta_0$	180×144×190	32
			260^+	155^+	520^+		
6	2652	6.98	$2.16\delta_0$	$1.3\delta_0$	$3.68\delta_0$	180×128×200	19
			229^+	137^+	390^+		

The computation at $M_\infty = 4.5$ was first performed. The TDNS of a subharmonic transition process at $M_\infty = 4.5$ (Adams, 1993) was continued until the flow has gone through the breakdown stage and become turbulence. Then the TDNS transition data were used as the initial solution to start the spatial marching with the approach described in §2. Since the TDNS transition data are not the solutions of the Reynolds-average Navier-Stokes equations, spatial transients are expected in the first few steps. Usually, the transients diminish after a few steps. The spatial extent affected by the transient solutions depends on both the character of the Reynolds-averaged Navier-Stokes equations and the initial conditions. This issue is beyond the scope of this report.

All computations are performed on a NEC-SX3 computer with one processor, with the code running typically at 1.8 GFLOPS. To cut down computation cost, a smaller box was used at the first step, and the solution is advanced in time until a statistically steady-state is reached. Then the solution was marched downstream one step spatially with a bigger computation box. In the cases of $M_\infty = 3$ and 6, the solutions from the $M_\infty = 4.5$ case were first rescaled and used as the initial data to start the spatial marching. Similar to the case of $M_\infty = 4.5$, smaller boxes were used in the first two steps, and then a bigger box was used at the third step.

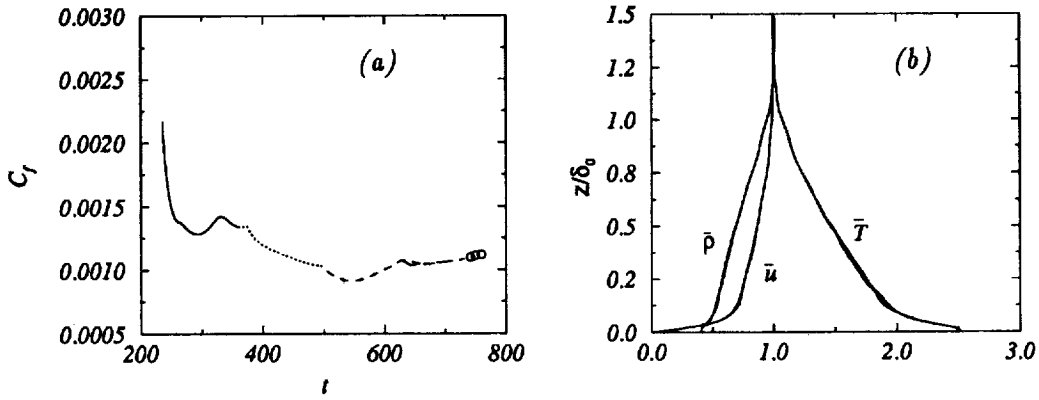

FIGURE 1. (*a*) Time history of skin friction coefficient, C_f. Legend: —— step 1; ····· step 2; ---- step 3; -·- step 3 with a big box; o sampling period. (*b*) Mean profiles of $\overline{u}$, $\overline{T}$ and $\overline{\rho}$ at $M_\infty = 3$ over $t = 438 - 472$. The profiles at $t = 472$ are indicated by —— .

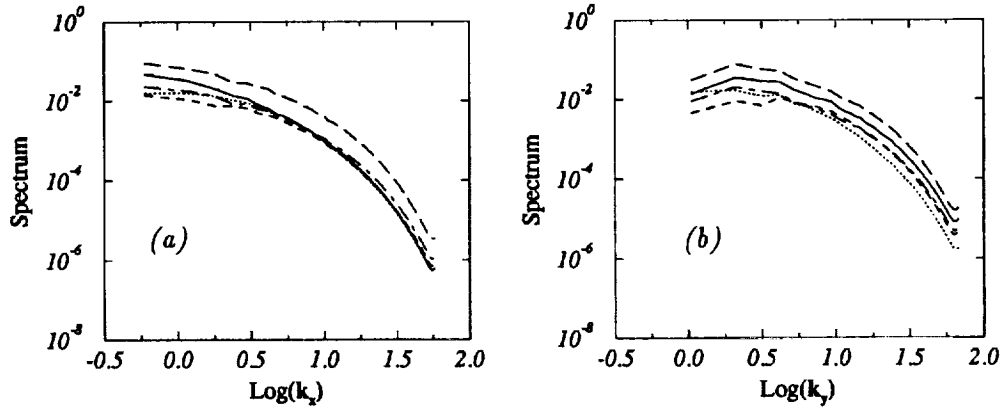

FIGURE 2. One-dimensional spectra of $\mathbf{u}'$ at $z = 30^+$ and $M_\infty = 3$: (*a*) in the x direction; (*b*) in the y direction. Legend: —— u; ····· v; ---- w; —— T; -·- ρ.

Fig. 1(*a*) shows the time history of skin coefficient, C_f, during the first three steps at $M_\infty = 6$. Here t is non-dimensionalized by the free-stream quantities. It can be seen that at each station, C_f is able to reach a statistically steady state. The data presented in this report is taken from the third step. At the first step, a large variation of C_f is observed. We believe this is due to the large transient caused by the initial conditions. Note that the initial data is rescaled from that of $M_\infty = 4.5$ case. A similar pattern has also been observed at $M_\infty = 3$.

Fig. 1(*b*) shows the variations of the mean profiles, $\overline{u}$, $\overline{T}$ and $\overline{\rho}$ over the time period $438 - 472$ at $M_\infty = 3$. It can be seen that though the boundary layer does not grow with t, it does vary with t. We expect that the fluctuations of the mean flow quantities with time will become smaller when a bigger computational box is used.

In all cases, one-dimensional spectrum is monitored to ensure that the computations are well resolved. Fig. 2 shows the one-dimensional spectra near the wall at $M_\infty = 3$. Here the wavenumbers, k_x and k_y, are normalized by the boundary layer thickness. It can be seen that in both plots, the difference between maximum and minimum spectral components is maintained to be at least $10^{3.5}$ to 10^4. Similar situations are found in the cases of $M_\infty = 4.5$ and 6.

Figs. 3-5 show the two-point correlations for all three cases. Compared to incompressible channel or boundary layer simulations (Kim *et al.*, 1987 and Spalart, 1988), the values of these functions are too high near the centers of the boxes. A similar situation was also reported in the compressible channel simulations of Coleman *et al.* (1993). In Coleman *et al.* (1993), acoustic effects are found to be responsible for high correlations observed in the compressible channel flows. Here this issue has not been investigated thoroughly so far. In all our cases, rather large streaks have been observed (cf. §4.2). We speculate that the existence of these large streaks near the wall might be the primary reason for the high two-point correlations.

Note that the downstream developments of the solutions have not been investigated in this study, since such investigations require the solutions to be marched downstream a few steps. So far we have only marched the solution downstream three steps at most. The solutions at these steps might still be affected by the spatial transients.

4.2 Large streamwise streaks

In all cases, large streamwise streaks have been observed. Fig. 6 shows the contour surface of $\overline{u} = 0.4$ at $M_\infty = 3$. In the figure, the spanwise dimensions of the streaks are about 100^+, which are close to those found in an incompressible boundary layer flow. The streamwise dimension of these streaks cannot be obtained from the figure since the computational box is not large enough. Fig. 7 gives an impression of the extent of these streaks in the wall-normal direction. Compared to the boundary layer thickness ($\delta_0 = 314^+$), they are rather large, affecting almost one third of the boundary layer.

Figs. 8 and 9 show a similar situation at $M_\infty = 4.5$, except that here the streaks are even bigger compared to the boundary layer thickness ($\delta_0 = 163^+$). So far we have not been able to study the spanwise and streamwise extents of these streaks systematically, primarily due to the their large size together with the present limitation to small computational boxes (in terms of wall units). Since these streaks are rather large compared to the computational boxes, their evolution affect both mean flow quantities $\mathbf{u}^0$ and turbulence quantities $\mathbf{u}'$ (note that $\mathbf{u}'$ is solved from (19) correctly only if $\mathbf{u}^0$ is steady). Thus the quality of our DNS data needs still to be assessed, and readers should be aware of that in comparing our DNS results with other sources.

The mechanism for the formation of these large streaks are not clear to us. In compressible channel flows, DNS results have shown that compressibility effects may be responsible for rather large structures in the streamwise directions (Coleman *et al.*, 1993, Coleman, 1993 and Moser, private communication, 1994). In our cases, we speculate that both compressibility effects and low Reynolds number effects due to

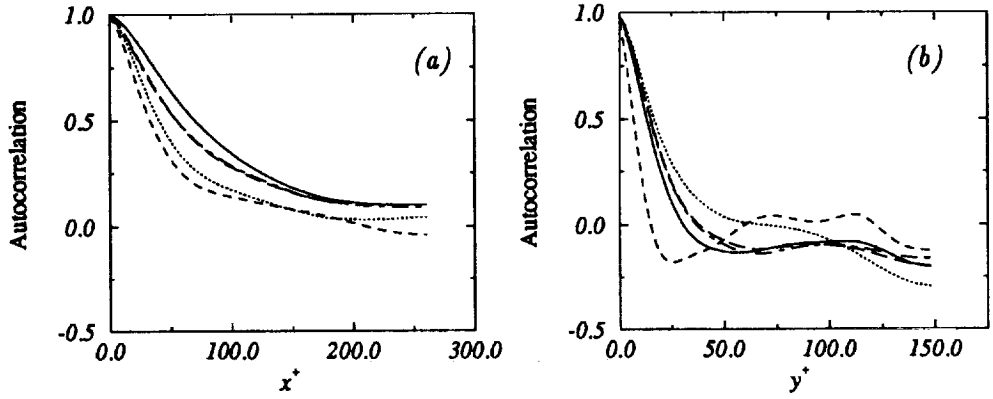

FIGURE 3. Two-point correlations at $z = 18.8^+$ and $M_\infty = 3$: (a) in the x direction; (b) in the y direction. Legend: —— u; ····· v; - - - - w; —— T; -·-· ρ.

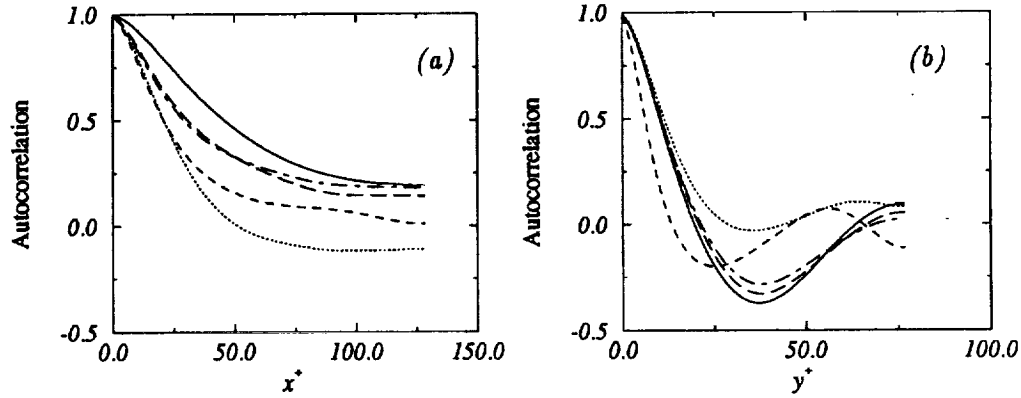

FIGURE 4. Two-point correlations at $z = 17.3^+$ and $M_\infty = 4.5$: (a) in the x direction; (b) in the y direction. Legend is the same as Fig. 3.

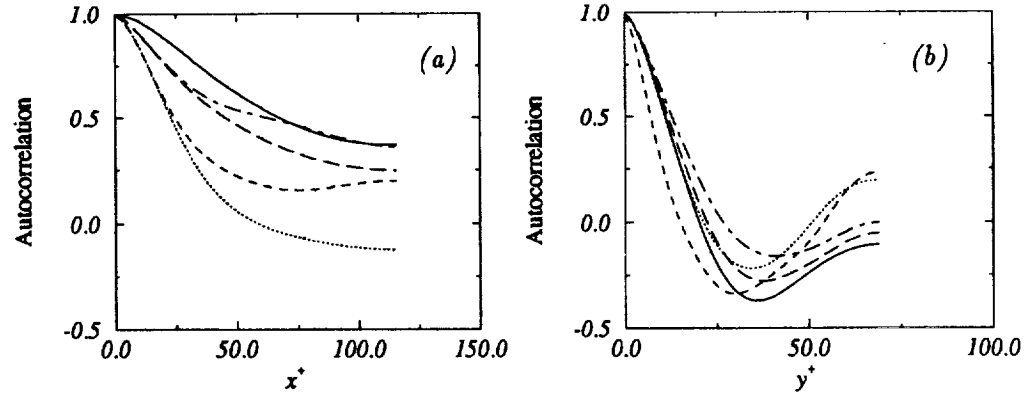

FIGURE 5. Two-point correlations at $z = 15.6^+$ and $M_\infty = 6$: (a) in the x direction; (b) in the y direction. Legend is the same as Fig. 3.

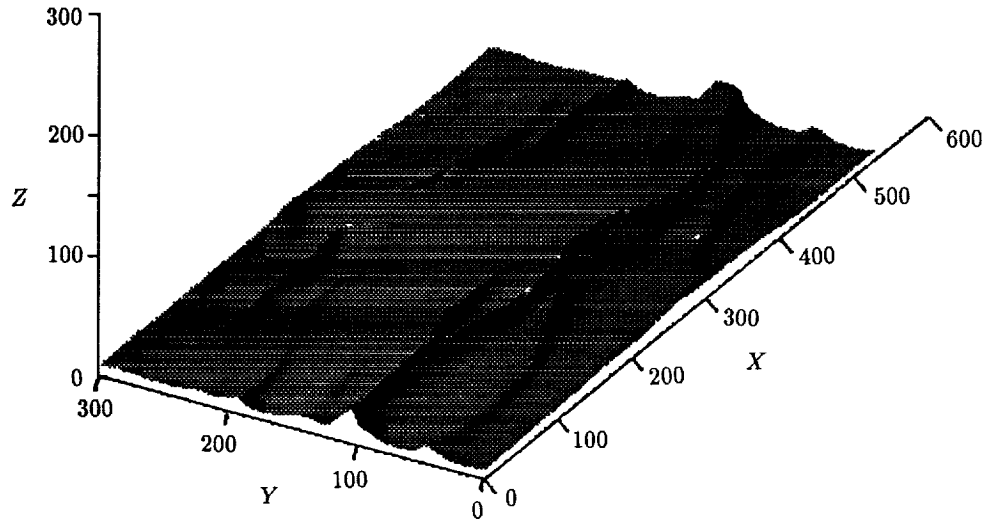

FIGURE 6. Contour surface of $\overline{u} = 0.4$ at $M_\infty = 3$.

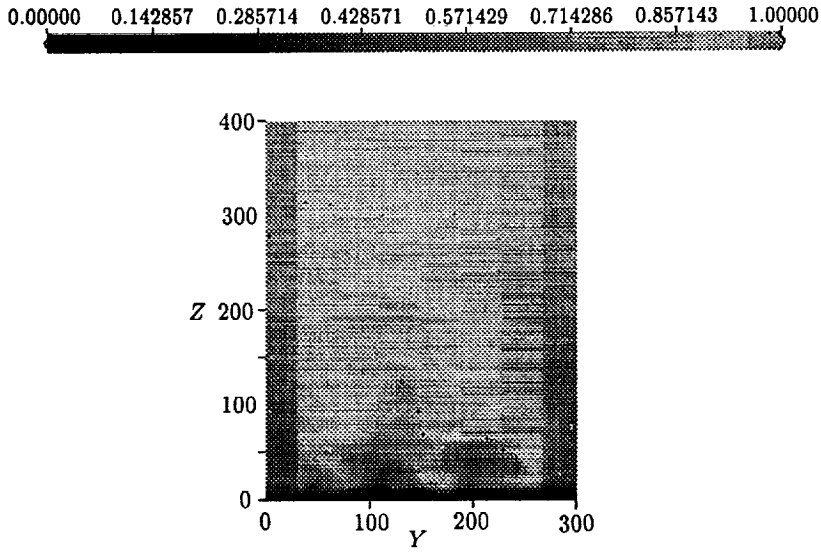

FIGURE 7. Contour plot of $\overline{u}$ on the $y - z$ plane at $x = 0$ and $M_\infty = 3$.

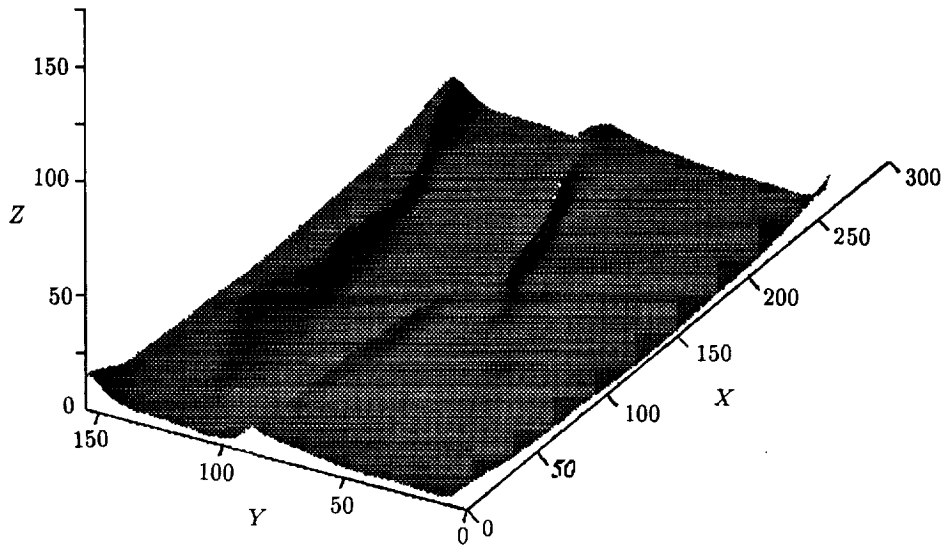

FIGURE 8. Contour surface of $\overline{u} = 0.3$ at $M_\infty = 4.5$.

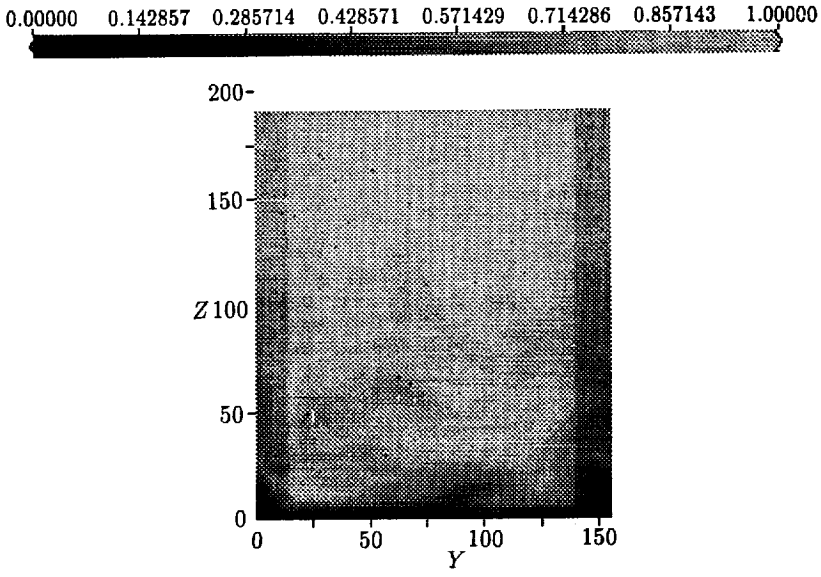

FIGURE 9. Contour plot of $\overline{u}$ on the $y - z$ plane at $x = 0$ and $M_\infty = 4.5$.

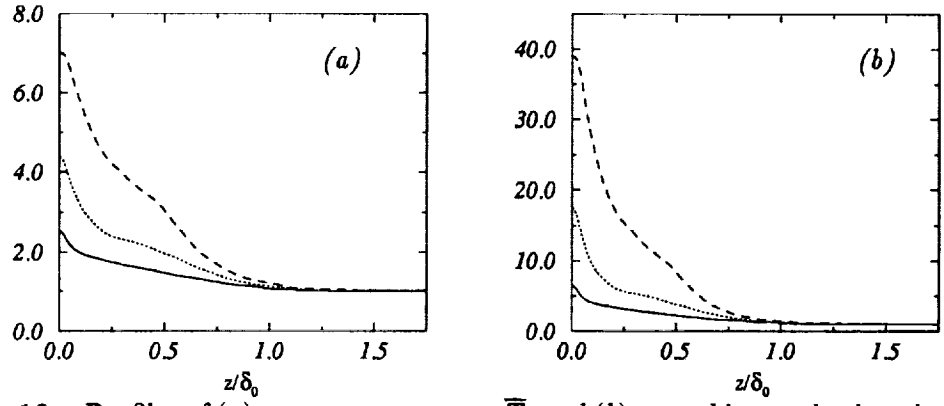

FIGURE 10. Profiles of (a) mean temperature, $\overline{T}$, and (b) mean kinematic viscosity, $\overline{\nu}$. Legend: —— $M_\infty = 3$, ····· $M_\infty = 4.5$, ---- $M_\infty = 6$.

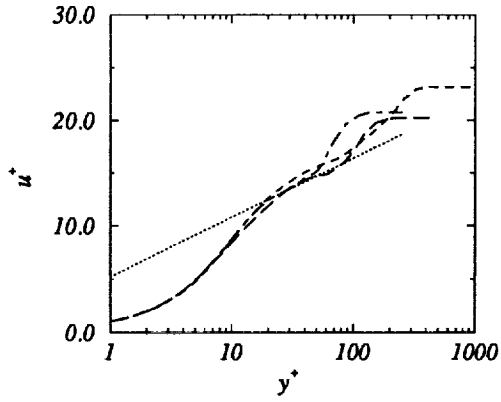

FIGURE 11. Mean streamwise velocity, $\overline{u}$, after Van Driest transformation. Legend: ---- $M_\infty = 3$, —— $M_\infty = 4.5$, -·- $M_\infty = 6$, ····· $2.44\ln(y^+) + 5.5$.

hot-wall conditions may play important roles. With an increase in wall temperature, the density of air decreases and its viscosity increases. This effectively reduces the Reynolds number in the near wall region. Fig. 10(a) shows the averaged temperature profiles across the boundary layers at different Mach numbers. The corresponding profiles for the kinematic viscosity, $\overline{\nu}$, are shown in Fig. 10(b). It can be seen that the increase of $\overline{\nu}$ is roughly proportional to $\overline{T}^2$. Therefore, the reductions of effective Reynolds numbers in the near wall regions due to the hot-wall conditions are significant.

4.3 Mean flow quantities

Fig. 11 shows the streamwise velocity profiles after the Van Driest transforms. Here the Van Driest transformation is defined by

$$\overline{u}^+_{VD} = \int_0^{\overline{u}^+} \left(\frac{\overline{\rho}}{\rho_w}\right)^{\frac{1}{2}} d\overline{u}^+ .$$

It can be seen that in all three cases, there are no apparent log-law regions. Note that at similar Reynolds numbers, some log-law regions can be observed in incompressible boundary layer flows (cf. Spalart, 1988). Thus we may conclude that the low Reynolds number effects due to the hot-wall conditions in our cases are significant.

Table 2 shows the skin friction coefficients, in comparison with the results of Van Driest transformation II, computed by Zeman (1993) at $Re_\theta = 10000$. Note that the Van Driest transformation II is usually formulated in terms of Re_x. Due to the difficulty in converting Re_x to Re_θ for a compressible turbulent boundary layer, we did not compute C_f at the relevant Re_θ so far.

TABLE 2. Computed skin friction coefficients compared to the calculations of Zeman (1993) using Van Driest transform II at $Re_\theta = 10000$.

M_∞	$C_f \times 10^{-3}$	C_f/C_{fi}	Van Driest II
3	1.854	0.522	0.58
4.5	1.729	0.470	0.40
6	1.110	0.303	0.30

Due to significant low Reynolds number effects in our DNS data, the effectiveness of Van Driest transformation cannot be demonstrated in this report. Readers are referred to Huang & Coleman (1994) for a further discussion on this issue.

4.4 Compressibility effects

Fig. 12 shows the profiles of turbulent Mach numbers. Note that M_t does not increase to the value that one would expect at $M_\infty = 6$. We believe that this is primarily due to the higher wall temperature at $M_\infty = 6$. We have seen in Fig. 10(b) that the kinematic viscosity, $\overline{\nu}$, is roughly proportional to $\overline{T}^2$. A lower than expected M_t at $M_\infty = 6$ is presumably caused by the high $\overline{\nu}$, which damps out the fluctuations in the near wall region.

In homogeneous flows, compressibility effects in the turbulent kinetic energy (TKE) equation can be measured by the dilatational dissipation, $\overline{\rho}\epsilon_d = \frac{4}{3}\overline{\mu u'^2_{i,i}}$, and the pressure-dilatation correlation, $p_d = \overline{pu'_{i,i}}$ (cf. Friedrich, 1993, Sarkar,1993, Spina *et al.*, 1994 and Lele, 1994 for a review). Recent work by Huang *et al.* (1994) also indicates that this is true for the near-wall turbulence. The inhomogeneous terms resulted from the compressibility of fluid are small and confined to the region very close to the wall. In Fig. 13, we have plotted these two terms, in comparison to the incompressible part of the dissipation, solenoidal dissipation $\overline{\rho}\epsilon_s = \overline{\mu\omega'_i\omega'_i}$, where ω_i is the component of vorticity. It can be seen that in all three cases, these two terms are small compared to solenoidal dissipation, $\overline{\rho}\epsilon_s$. This indicates that the influence of fluid compressibility on TKE is rather small in the flat plate boundary layer flows investigated here. Similar observations are also made by Huang *et al.* (1994) for near-wall turbulence in compressible channel flows at Mach number 3, and by Dinavahi & Pruett (1993) and Adams (1993) for late stage transitional boundary layer flows at $M_\infty = 4.5$.

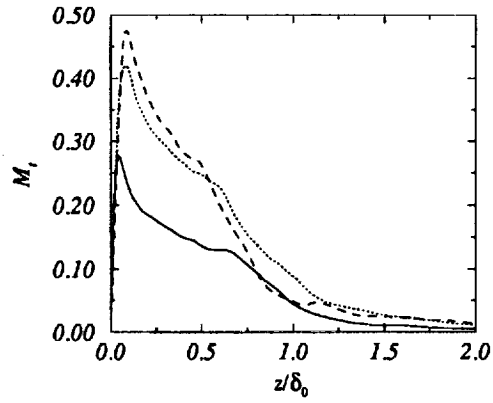

FIGURE 12. Turbulent number Mach number, $M_t = M_\infty \sqrt{\widetilde{u_i'' u_i''}}/\sqrt{\widetilde{T}}$. Legend: —— $M_\infty = 3$, ····· $M_\infty = 4.5$, ---- $M_\infty = 6$.

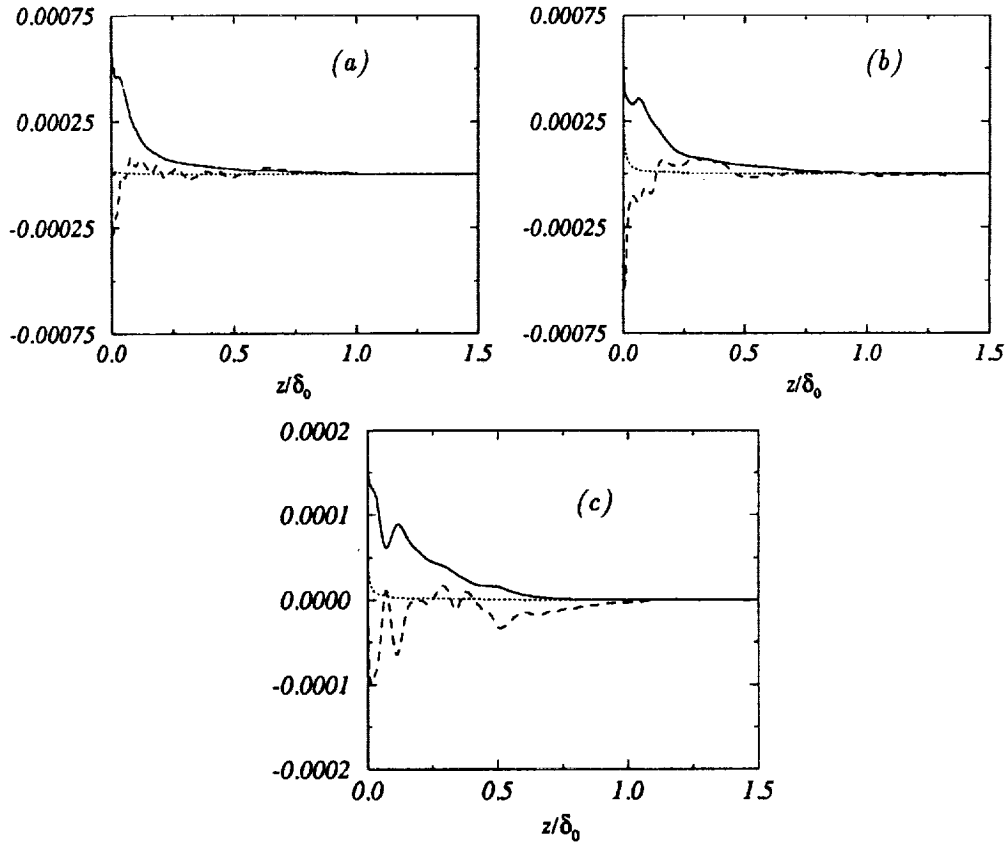

FIGURE 13. Compressibility effects: —— solenoidal dissipation, $\overline{\rho}\epsilon_s$, ····· dilatational dissipation, $\overline{\rho}\epsilon_d$, ---- pressure-dilatation correlation, p_d. (*a*) $M_\infty = 3$. $\overline{\rho}\epsilon_d$ and p_d have been enlarged 100 times. (*b*) $M_\infty = 4.5$. $\overline{\rho}\epsilon_d$ and p_d have been enlarged 10 times. (*c*) $M_\infty = 6$. $\overline{\rho}\epsilon_d$ and p_d have been enlarged 10 times.

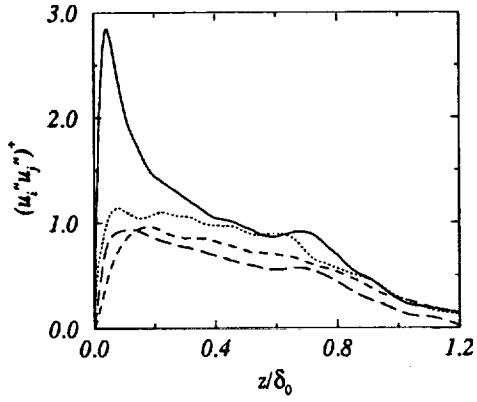

FIGURE 14. Favre-averaged Reynolds stress terms normalized by wall unit: —— $u''u''$; ····· $v''v''$; ---- $w''w''$; and —— $u''w''$.

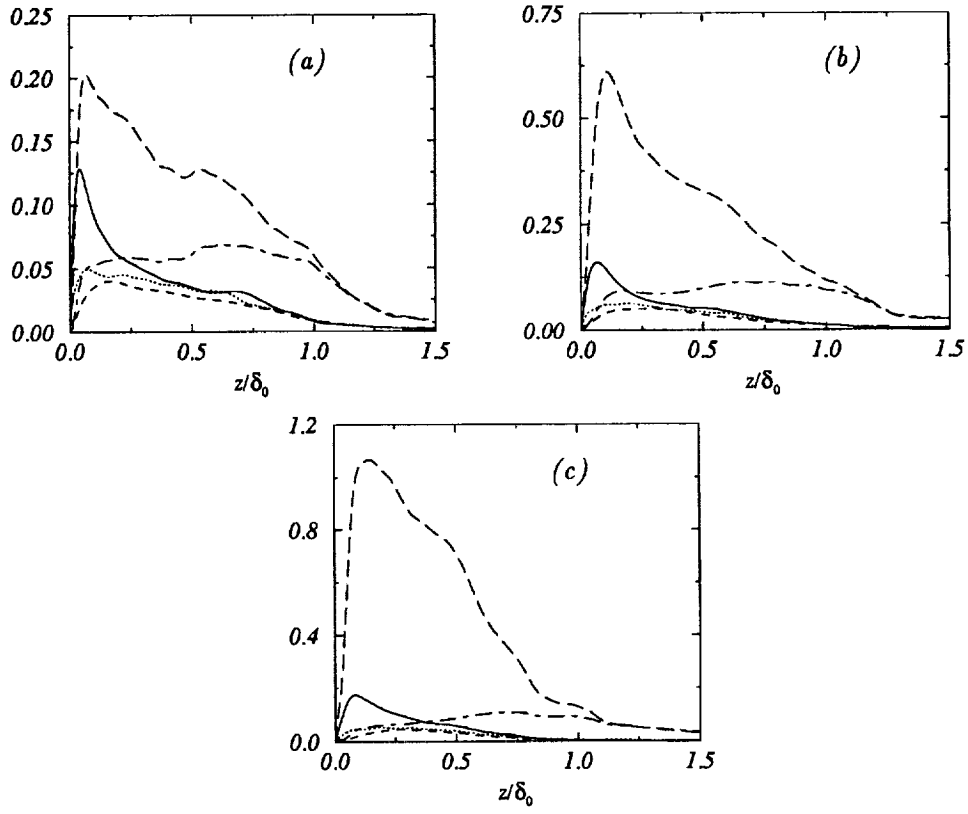

FIGURE 15. The *r.m.s.* of turbulence quantities: —— u', ····· v', ---- w', —— T', -·- ρ'. (*a*) $M_\infty = 3$; (*b*) $M_\infty = 4.5$; (*c*) $M_\infty = 6$.

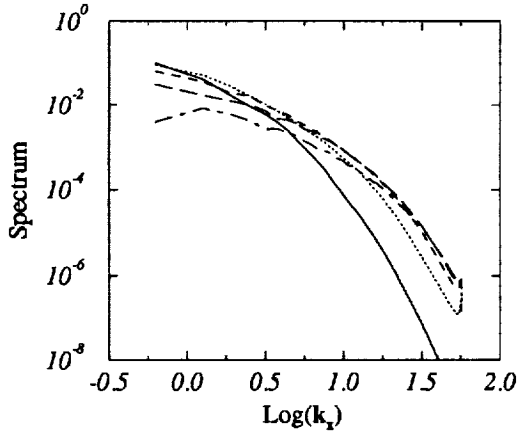

FIGURE 16. Spectra of u in the x direction taken from $z/\delta_0 = 0.04$ ——— , 0.1 ····· , 0.16 ---- , 0.42 —— , and 0.85 -·- at $M_\infty = 4.5$.

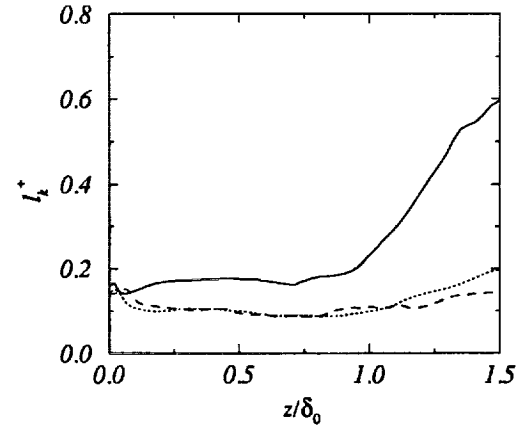

FIGURE 17. Kolmogorov scales, l_k^+, normalized by wall unit. Legend: ——— $M_\infty = 3$, ····· $M_\infty = 4.5$, ---- $M_\infty = 6$.

4.5 Other quantities

Since our DNS data are severely affected by low Reynolds number effects, large streaks, and small computational boxes, we do not expect to get good statistics in all three cases. In this subsection, we shall only present a few basic quantities to give readers a qualitative impression.

The Favre-averaged Reynolds stress terms normalized by the wall units at $M_\infty = 3$ are shown in Fig. 14. Fig. 15 shows the turbulence fluctuation $\mathbf{u}'$ for the three cases. It can be seen that the density fluctuations, ρ', have larger amplitudes near the edges of the boundary layers in all three cases.

5. Discussions

In all our computations, the computational boxes are rather small in terms of wall units, but not small at all in terms of boundary layer thickness. That is due to the fact that the hot-wall conditions increase the wall units in terms of boundary layer thickness. Apparently for the cases studied in this report, larger boxes are needed in order to give improved turbulence statistics. This, however, is expected to be computationally very expensive if the resolution used in this study is to be kept. One may argue that coarser grids might be sufficient since the hot-wall conditions reduce the effective Reynolds number in the near wall region and turbulence scales are large away from the walls. This argument is not supported by our numerical experience so far. Fig. 16 shows the one-dimensional spectra taken at different distances from the wall at $M_\infty = 4.5$. It can be seen that the spectra have almost the same value at high wavenumber from $z/\delta_0 = 0.21$ to 0.85. This indicates that the resolution requirement is not reduced at all away from the wall. In order to find the explanation, we plot in figure 17 the Kolmogorov scale, l_k^+, as functions of z. In the figure, we can see that l_k^+ has roughly the same value in most part of the boundary layer. Similar situations can be seen in $M_\infty = 3$ and 6 cases. Since one needs rather dense grids in the near wall region to resolve mean flow profiles, the resolution requirement may be more or less the same throughout the whole boundary layer. This observation is basically supported by the one-dimensional spectra in Fig. 16. Apparently, this situation is rather different from that in incompressible boundary layer flows, where dense grids are needed only in the near wall region. From the above discussion, we can conclude that turbulent boundary layers with hot-wall conditions require a larger computational effort than in the cold-wall case.

In Fig. 17, one can also see that l_k^+ is much smaller than that in an incompressible fluid case, where $l_k^+ \approx 2^+$ (Moser, private communication, 1994). This suggests that the grid spacing rules derived from DNS of incompressible boundary layer flows cannot be applied to a compressible flow case.

6. Concluding remarks

In this report, we have presented a numerical approach for DNS of compressible turbulent boundary layer flows, which solves the parabolized Reynolds-average Navier-Stokes equations for mean flow quantities and computes turbulence quantities locally with a temporal DNS approach. Preliminary results from three cases at $M_\infty = 3$, 4.5, and 6 are presented. All our results indicate that compressibility effects on turbulent kinetic energy equations, i.e. dilatational dissipation and pressure-dilatation correlation, are small. Due to the hot-wall conditions used in all cases, these preliminary results are severely affected by low Reynolds number effects, large streaks, and small computational boxes. Hot-wall conditions seem to be more difficult to deal with than cold-wall conditions. Grid spacing rules derived from the DNS of incompressible boundary flows are not valid in a compressible case.

Acknowledgments

We gratefully acknowledge the invaluable discussions with Dr. Kleiser during the

course of this work. Thanks are due Drs. G. A. Blaisdell, P. Bradshaw, G. N. Coleman, P. G. Huang, R. Moser, M. Rai, and O. Zeman for their many helpful comments and suggestions during the 1994 summer program at CTR.

REFERENCES

ADAMS, N. A. 1993 Numerische Simulation von Transitionsmechanismen in kompressiblen Grenzschichten . *Doctoral Dissertation,* Technical University of Munich, Germany. Also DLR-FB 93-29, DLR, Germany (in German).

BERTOLOTTI, F. P., HERBERT, TH. & SPALART, P. R. 1992 Linear and nonlinear stability of the Blasius boundary layer. *J. Fluid Mech.* **242,** 441-471.

COLEMAN, G. N., BUELL, J. G., KIM, J. & MOSER, R. D. 1993 Direct simulation of compressible wall-bounded turbulence. *Proc. 9th Symp. on Turbulent Shear flow.* Kyoto, Japan.

COLEMAN, G. N. 1993 Direct simulation of isothermal-wall supersonic channel flow. *CTR Annual Research Briefs 1993.*Center for Turbulence Research, Stanford Univ./NASA Ames Research Center, 313-328.

FLETCHER, C. A. J. 1988 *Computational Techniques for Fluid Dynamics, Volume II.* Springer-Verlag, Berlin.

FRIEDRICH, R. 1993 Compressible turbulence. *Space Course 1993.* Technical University of München, Germany.

GUO, Y., ADAMS, N. A. & KLEISER, L. 1994 Modeling of nonparallel effects in temporal DNS of compressible boundary layer transition . *Theoret. Comput. Fluid Dynamics.* in press.

GUO, Y. & FINLAY, W. H. 1994 Wavenumber selection and irregularity of spatially developing Dean and Görtler vortices . *J. Fluid Mech.* **264,** 1-40.

HAIRER, E., NØRSETT, S. P. & WANNER, G. 1987 *Solving Ordinary Differential Equations I.* Springer-Verlag, Berlin.

HUANG, P. G. & COLEMAN, G. N. 1994 Van Driest transformation and compressible wall-bounded flows. *AIAA J.* in press.

HUANG, P. G., COLEMAN, G. N. & BRADSHAW, P. 1994 Compressible turbulent channel flows - a closer look using DNS data. Submitted for publication.

KIM, J., MOIN, P. & MOSER, R. 1987 Turbulence statistics in fully developed channel flow at low Reynolds number. *J. Fluid Mech.* **177,** 133-166.

KLEISER, L. & ZANG, T. A. 1991 Numerical simulation of transition in wall-bounded shear flows. *Ann. Rev. Fluid Mech.* **23,** 495-537.

LELE, S. L. 1994 Notes on the effects of compressibility on turbulence. *Ann. Rev. Fluid Mech.* **26,** 211-254.

SARKAR, S. 199 Turbulence modeling and simulation of high-speed flows. *Space Course 1993.* Technical University of München, Germany.

SPALART, P. R. & LEONARD, A. 1985 Direct numerical simulation of equilibrium turbulent boundary layers. *Proc. 5th Symp. on Turbulent Shear Flows*. Ithaca, NY.

SPALART, P. R. 1986 Numerical study of sink-flow boundary layers. *J. Fluid Mech.* **172,** 307-328.

SPALART, P. R. 1988 Direct simulation of a turbulent boundary layer up to $Re_\theta = 1410$. *J. Fluid Mech.* **187,** 61-98.

SPALART, P. R. & WATMUFF, U. H. 1993 Experimental and numerical study of turbulent boundary layer with pressure gradients. *J. Fluid Mech.* **249,** 337-371.

SPINA, E. F., SMITS, A. J. & ROBINSON, S. K. 1994 The physics of supersonic turbulent boundary layers. *Ann. Rev. Fluid Mech.* **26,** 287-319.

ZANG, T. A. 1991 Numerical simulation of the dynamics of turbulent boundary layers: perspective of transition simulator. *Phil. Trans. R. Soc. Lond. A.* **337,** 95-102.

ZEMAN, O. 1993 A new model for super/hypersonic turbulent boundary layers. *AIAA Paper* 93-0897.